

# Void Detection in Complex Geometries

H. T. Banks<sup>1</sup>, N. L. Gibson<sup>2</sup>, and W. P. Winfree<sup>3</sup>

<sup>1</sup>Center for Research and Scientific Computation, Box 8205, North Carolina State University, Raleigh, NC 27606-8205

<sup>2</sup>Department of Mathematics, Kidder Hall 368, Oregon State University, Corvallis Oregon 97331-4605

<sup>3</sup>NASA Langley Research Center, MS 231, Hampton, VA 23681-2199

May 6, 2008

## Abstract

We present results from our computational efforts to determine defect characteristics via solution of inverse problems which involve the 2D wave equation in a domain which presents geometric complexities. We develop a technique for determining “optimal” placement of a receiver based on the geometry of the interrogation problem which involves a plane wave pulse and single receiver. A forward simulation of a scenario with an anticipated void is compared to a voidless scenario in a least squares sense to obtain a “visibility map” of the computational domain. The determined placement of the receiver is shown to be effective in reducing optimization iterations for a particular example.

## 1 Introduction

The particular motivation for this research is the detection of defects in the insulating foam on the space shuttle fuel tanks in order to help eliminate the separation of foam during shuttle ascent. The foam on the space shuttle is sprayed on in layers. Voids occur between layers. As the top of each layer cures, a thin knit line is formed which is of higher density (i.e., is comprised of smaller, more tightly packed polyurethane cells).

Pulsed THz frequency signals are being used in an interrogation procedure to detect voids in foam [BGW05]. The experiments are single source, single receiver, and the angle of incidence is non-normal. The particular case of detection of a void behind an obstacle, for instance a cylindrical bolt, is of great importance.

Current approaches to void detection using THz interrogation involve signal processing techniques which use time-of-flight data and peak-to-peak distance. Our intention is to apply a physics-based inverse problem formulation to the problem of damage characterization. In this report we address the specific task of choosing proper placement of the receiver to maximize potential detection in this formulation. In essence, we use the initial cost functional at all points in space to make this determination.

The outline of the paper is as follows. Section 2 discusses the modeling approach used in the forward problem. Section 3 defines the inverse problem formation for the void characteristics. Sections 4 and 5 give results for the non-obstructed case and obstructed case, respectively. Section 6 offers concluding remarks.

## 2 Mathematical Model

In modeling the interrogation problem of interest, several physical characteristics must be considered. First, note that the microstructure of the foam is smaller than the wavelength of the interrogating source. This, coupled with the fact that the domain is very large compared to wavelength, means that it is computationally impractical to represent the fine scale of the microstructure. Thus we must assume that we have a uniform material with constant dielectric parameters. One justification is that we may apply homogenization techniques to obtain an effective permittivity based on a complex microstructure [BBC<sup>+</sup>06].

We assume uniformity in the  $z$  direction so that our problem reduces to two spatial dimensions. We wish to further simplify our computations by assuming a constant (i.e., frequency independent) wave speed. Thus Maxwell's equations for the propagation of the electromagnetic field reduces to the 2D wave equation.

Lastly, in most THz experiments, the source signal is very broad band. However as we have already chosen a constant wave speed, this is unnecessary, and cumbersome for visualization. Therefore we will use (a "smooth" version of) a half-cycle pulse of a sine wave as the interrogating signal. Propagation will be in the  $x$  direction (uniform in  $y$ , thus a plane wave).

## 2.1 Equations and Boundary Conditions

We assume the electric field to be polarized in the  $z$  direction, thus for  $\vec{E} = (0, 0, E)$  and  $\vec{x} = (x, y)$  the propagation of the electric field can be modeled

$$\epsilon(\vec{x}) \frac{\partial^2 E}{\partial t^2}(t, \vec{x}) - \nabla \cdot \left( \frac{1}{\mu(\vec{x})} \nabla E(t, \vec{x}) \right) = -\frac{\partial J_s}{\partial t}(t, \vec{x})$$

where  $\epsilon(\vec{x})$  and  $\mu(\vec{x}) = \mu_0$  are the dielectric permittivity and permeability, respectively. Note that the permittivity is spatially dependent in the sense that it holds a constant value in the foam, and is constant in air. As we are neglecting magnetic effects we use the permeability of free space everywhere. In equation (2.1) the source current is given as

$$J_s(t, \vec{x}) = \delta(x) e^{-((t-t_0)/t_0)^4},$$

where  $t_0 = t_f/4$  when  $t_f$  is the period of the interrogating pulse. We use this function rather than a truncated sine for its differentiability. We choose homogeneous initial conditions  $E(0, \vec{x}) = 0$  as the electric field will be completely generated by the source signal.

The interrogation problem that we are considering involves a foam slab in front of (affixed to) a reflective aluminum backing. This provides a very natural boundary condition. However, our other three boundaries are artificial, and therefore must have boundary conditions which mimic an infinite domain. Thus, we define our finite computational domain to be  $\Omega = [0, 0.1] \times [0, 0.2]$ . On to the boundaries, we apply the following conditions:

- Reflecting (Dirichlet) boundary conditions (right)

$$[E]_{x=0.1} = 0$$

- First order absorbing boundary conditions (left)

$$\frac{\partial E}{\partial t} - \sqrt{\frac{1}{\epsilon(\vec{x})\mu_0}} \frac{\partial E}{\partial x} \Big|_{x=0} = 0$$

- Symmetric boundary conditions (top and bottom)

$$\left[ \frac{\partial E}{\partial y} \right]_{y=0, y=0.2} = 0$$

Note that this representation of the reflecting boundary condition is for the particular case when we have a normal angle of incidence, i.e., the aluminum backing is parallel to the  $y$  axis. It should be understood that for a non-normal incidence angle, the domain tilts so that the plane wave remains parallel to the  $y$  axis, thus the Dirichlet boundary condition becomes

$$[E]_{y=mx+b} = 0$$

where  $m$  represents the slope of the backing, and  $b$  is such that the backing is as far to the right as possible while still within the original computational domain.

We may model the speed of propagation in the domain as

$$c(\vec{x}) = \frac{c_0}{n(\vec{x})} = \sqrt{\frac{1}{\epsilon(\vec{x})\mu_0}},$$

where  $c_0$  is the speed in a vacuum and  $n$  is the index of refraction of the material. Note that we assume any void inside the foam, as well as the region outside the foam, to be equivalent to a vacuum.

## 2.2 Numerical Discretization

In our forward simulations we choose to apply a second order (piecewise linear) finite element method on a rectangular grid for spatial discretization. This is coupled with a second order (centered) finite difference method for the temporal derivatives. The resulting linear system from exact integration of the basis functions is sparse, however we observed no significant increase in error (while a substantial increase in speed) when applying quadrature rules. Thus we use a mass lumping approach resulting in an explicit method. As a consequence of our rectangular grid, stair-stepping approximations must be used for all slanted and curved interfaces.

## 3 Void Inverse Problem

We now define the inverse problem for parameters which characterize a possible void inside the foam region. Assume we have performed an interrogation experiment and have collected electric field data,  $\hat{E}_i$  at  $S$  sample times  $t_i$  and from some point in space  $\mathbf{x} = \mathbf{x}^+$ . It is from comparisons to this data that we hope to determine information about the presence of a void.

Given a trial value  $q$  of characteristics of a void (e.g., the width  $w$  of an elliptical void), we can simulate the electric field in the computational domain at all times  $t_i$  corresponding to the data using the model and numerical methods from Section 2. Thus, we estimate the true value of the void parameters  $q^*$  by solving the following inverse problem:

Find  $q \in Q_{ad}$  such that the following objective function is minimized:

$$\mathcal{J}_1(q) = \frac{1}{2S} \sum_{i=1}^S |E(t_i, \mathbf{x}^+; w) - \hat{E}_i|^2,$$

where  $Q_{ad}$  is some set of admissible values (e.g., non-negative widths) of values of  $q$ .

The problem of minimizing this objective function is ill-posed, and it is only possible to solve with a good initial guess for  $q$  and sufficient information about  $q^*$  contained in  $\hat{E}$ . Thus, the choice of location for  $\mathbf{x}^+$  is crucial, especially in the presence of an obstacle that may block the transmission of information.

## 4 Non-obstructed Scenario

We consider a sample interrogation problem wherein a foam slab is interrogated by a plane wave pulse at a non-normally incident angle, as depicted in Figure 1. In the schematic of the domain, the dot-dashed line represents the foam/air interface. The dashed lines represent knit lines, although their distinct dielectric properties are ignored here (they are treated in [BG06b]). Their presence here is merely to illustrate the formation of the void. The elliptical pocket (5 mm wide) between the knit lines is a void, modeled by  $n = 1$ . The slanted back wall is the aluminum backing, modeled as a perfect conductor. Note that the plot window depicts a truncated computational domain so that we may more easily ignore the spurious boundary reflections.

The plot in Figure 1 is not of the electric field at all points in space at a given time, as in a snapshot (see [BG06b]). Rather, we have plotted a measure of the relative intensity at each point in space averaged over time. Specifically the plot depicts

$$\sum_{i=1}^S E(\vec{x}, t_i)^2 \approx C \int_0^T E(\vec{x}, t)^2 dt.$$

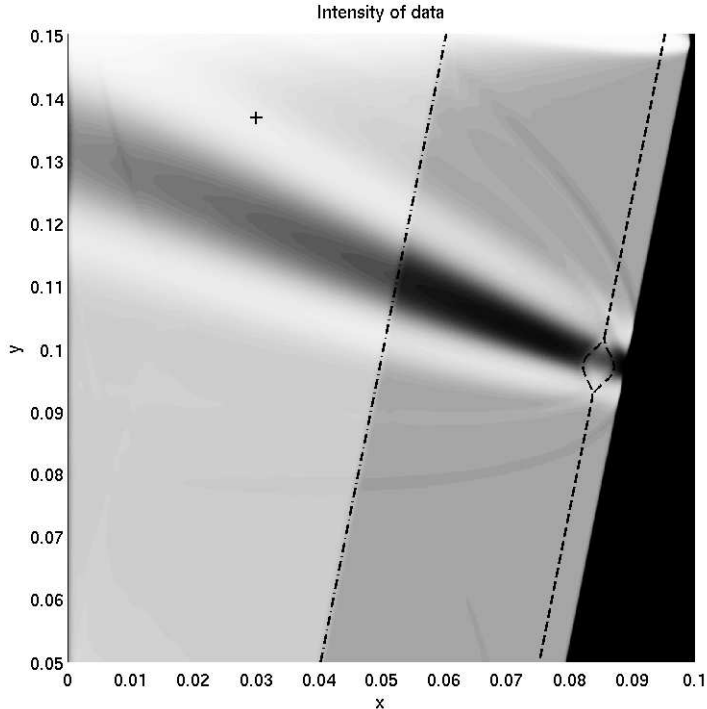


Figure 1: Intensity of data received from non-normally incident, plane wave interrogating material with a void. (Note: knit lines are ignored, dashed line is shown merely to highlight location of void.)

This representation can be thought of as a map of the total amount of information obtained by a receiver at any given point in space. In the sense of the inverse problem, we are interested in obtaining as much information as possible about the characteristics of the void. It is a natural question to ask then, whether there is a correlation between high intensity of the signal and high quality of information. In particular, there seem to be two distinct types of regions in the intensity map of Figure 1, the narrow band of low intensity, and the high intensity bands which flank it. To determine which of these regions should be preferred for the location of the source in an inverse problem formulation, we need to consider this information in the context of a least squares objective function.

The idea is that if the electric field values plotted in Figure 1 were data  $\hat{E}$  from an actual experiment, we would not be looking at the sum of  $\hat{E}(\vec{x}, t_i)^2$ , but instead the sum of the differences squared,

$$\sum_{i=1}^S |\hat{E}(\vec{x}, t_i) - E(\vec{x}, t_i; q)|^2. \quad (1)$$

While in an experimental setup, the location  $\vec{x}$  would be fixed, in a simulation we may consider all points in our computation domain. It is important to note that only a time marching solver on the entire domain of interest can be used to generate this information.

In Equation (1) the value of the parameter  $q$  would generally be chosen to be close to that corresponding to the expected void characteristics. However, here we are considered with the question of: when can any information be obtained? Thus we may choose  $q$  to represent no void at all (e.g.,  $w = 0$ ). Figure 2 depicts the sum of differences squared (e.g., Equation (1)) between the simulation with a void (as represented by the underlying schematic in the figure) and the simulation without a void. We refer to this type of plot as a visibility map as it allows a determination of whether a least squares objective function could detect the presence of a void with placement of the receiver at a particular coordinate.

In Figure 3 we depict the difference between the assumed data from a simulation with a void and data from a voidless simulation, when the receiver happens to be in the region of highest intensity (the location

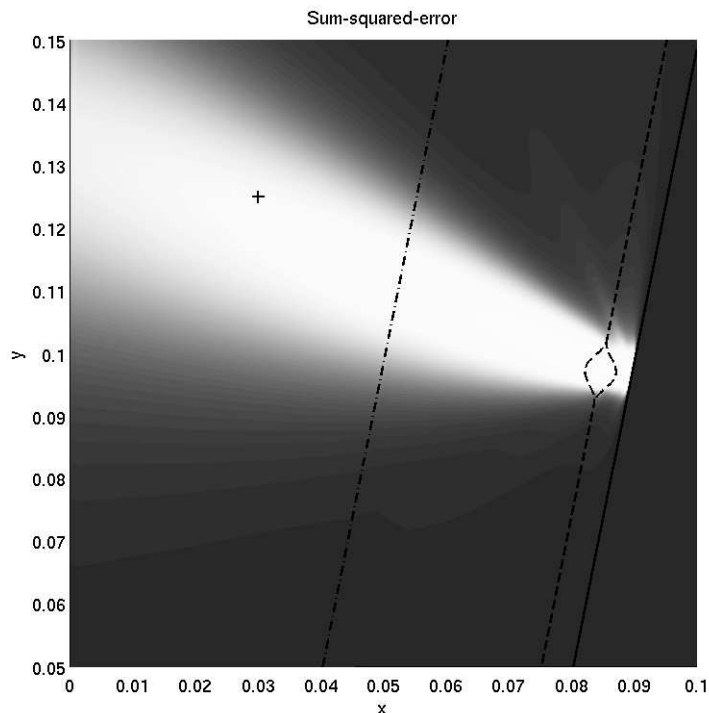


Figure 2: Shown is a surface plot of the objective function at  $w = 0$ . Cross denotes the location of a point in the region of least intensity in signal received (as determined by Figure 1). Note that it correlates with the region of greatest contrast between material with void and without.

of the “+” in Figure 1). The original signal peak is merely shown for reference. The inset axes contain a zoom of the primary reflection from the metallic backing.

We may compare Figure 3 to Figure 4 which contains a plot of the difference between the assumed data from a simulation with a void and data from a voidless simulation, when the receiver happens to be in the region of lowest intensity (the location of the “+” in Figure 2). We note that the amplitude of this difference is twice as high as that from the high intensity signal.

The conclusion is that the decrease in intensity as demonstrated by Figure 1 is due to the disruption of the interrogating plane wave by the presence of the void. In the regions where there is no such decrease in intensity, there is less information about the void. In this example there is a direct correlation between the intensity map and the visibility map. The situation becomes more complicated, however, with the inclusion of an obstacle.

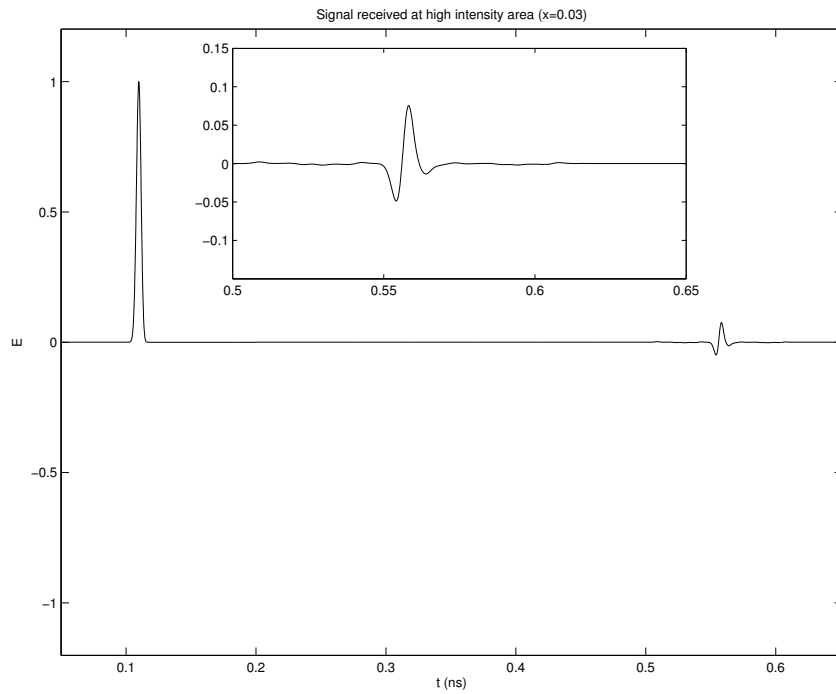


Figure 3: Shown is the difference between data received from non-normally incident, plane wave interrogating material *with and without a void* when receiver is placed in high intensity region. (Note: original signal peak is shown for reference.)

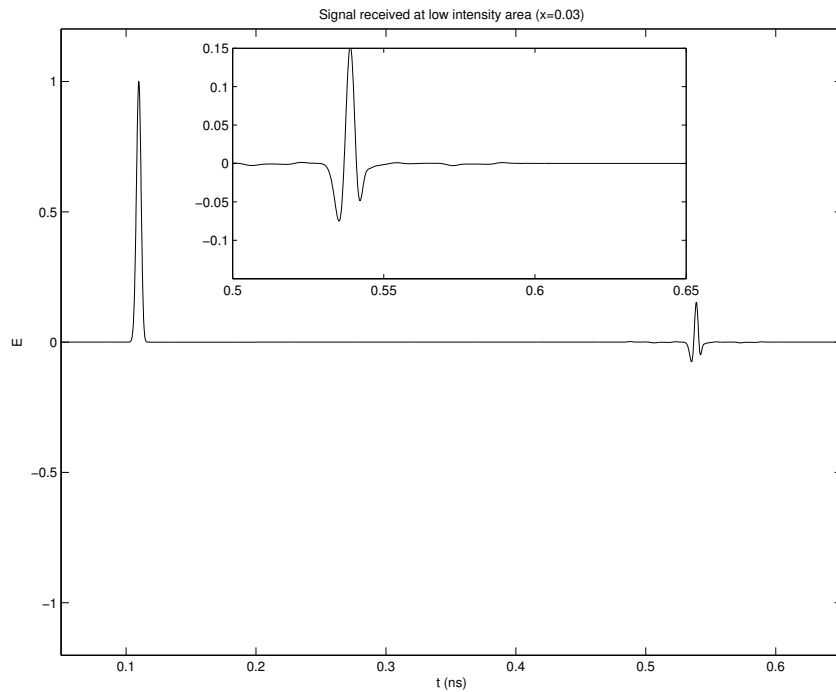


Figure 4: Shown is the difference between data received from non-normally incident, plane wave interrogating material *with and without a void* when receiver is placed in low intensity region. Amplitude of difference is doubled compared to high intensity region.

## 5 Obstructed Scenario

We consider a different sample interrogation problem involving a foam slab with a large circular (actually 3D cylindrical, but circular in 2D) obstacle, as shown in Figure 5. Again, the dot-dashed line in the schematic represents the foam/air interface and the dashed lines represent knit lines. The elliptical void is located just behind the obstacle, necessitating a non-normal angle of incidence or else nothing would be visible from outside the foam. The slanted back wall again is the aluminum backing, modeled as a perfect conductor.

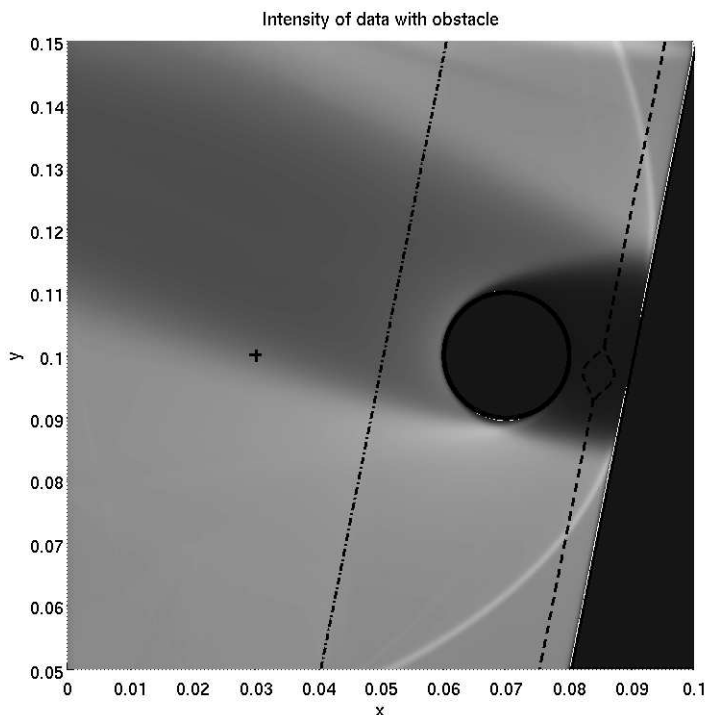


Figure 5: Intensity of data received from interrogating a material with an obstacle in front of a void.

The plot in Figure 5 depicts a measure of the relative intensity at each point in space averaged over time. Again, there seem to be two distinct types of regions in the intensity map. In this example there is again a band of low intensity, this time wider, flanked by regions of high intensity, although this time not as high.

Rather than demonstrate choices of location of the receiver in each of the low intensity region and the high intensity region, we choose two locations on the interface between intensity regions. In particular, one point (marked with a “+” in Figure 5) which is on the bottom of the low intensity region, and another which will be directly above the region. The reasoning for this choice of comparison will be made clear shortly.

In Figure 6 we show the difference between the assumed data from a simulation with a void and data from a voidless simulation, when the receiver is just below the low intensity region. The original signal peak is again shown for reference. The inset axes contains a zoom of the primary reflection from the metallic backing. Note the scale on the inset axes.

In Figure 7 we show the difference between the assumed data from a simulation with a void and data from a voidless simulation, when the receiver is just above the low intensity region. We observe that the scale of the inset axes is an order of magnitude higher. This implies that the contrast between the signal with a void and without is much higher from this receiver location than from directly below the low intensity region. However, we emphasize that the overall intensity levels of the two locations is equivalent. The important difference is the type of information contained in the signal, not the amount of information.

Figure 8 depicts the visibility map, i.e., the sum of differences squared between the simulation with a void (as represented by the underlying schematic in the figure) and the simulation without a void, for the

example of foam interrogation in the presence of an obstacle. The “+” in the plot denotes the position of the receiver referred to in Figure 7.

Now we can see clearly why the signal in Figure 7 had more information about the void than did the signal from Figure 6. While the latter was in a region of equivalent intensity, the signal that reached that position could not have gone through the void. As determined by the visibility map, that position is in a region of invisibility. However, the former position happens to correspond to the region of greatest visibility. The conclusion here is that there is no direct correlation between the intensity map and the visibility map in the presence of an obstacle.

Finally, we show a plot in Figure 9 of an objective function  $\mathcal{J}$  as a function of void width. For this particular example, the true value is  $w = 0.02$ . The two curves shown represent the two cases of choosing the location of the receiver above or below the low intensity region. The plot clearly shows a higher level of contrast in the curve marked “high” (meaning above the low intensity region). This optimization problem would be more likely to converge quickly, and would be less disrupted by the presence of noise.

## 6 Concluding Remarks

It is clear from this analysis that in a problem scenario involving plane wave interrogation without obstacles, receiver placement should be in region of low intensity for highest contrast (intensity is low due to void). However, the situation with obstacles is more complex. In the example herein the optimal receiver placement happened to be at the interface between regions of low and high intensity for highest contrast (intensity is lowered due to obstacle but relatively high due to information about the void). In general the balance between these two opposing concerns is not clear, and there is no direct correlation between the intensity map and the visibility map. One should make receiver placement decisions on the basis of the visibility map; however, the signal received must be strong enough itself to be differentiated from noise. We point out that the experimental practitioner can usually maximize intensity by hand (moving the sensors until the highest signal is received), but a visibility map must be simulated.

This work does not incorporate measurement noise (estimated to be  $\text{SNR} \approx 100:1$ ). The little information that escapes an obstacle may be further masked by measurement error. Additionally, note that if the angle of incidence were slightly increased in the obscured example, the preferred receiver position would be the one below the invisibility region instead of the one above. Therefore, if there is significant uncertainty in the angle of incidence, the qualitative information in the visibility map may not match the actual data. A fully robust procedure for determining optimal receiver placement in a void detection experiment must account for variability in the void sizes sought after, the geometry of the surrounding obstacles, and even the dielectric parameters of the material (see for example [BG06a]).

## Acknowledgements

This research was supported in part by NASA under grant NIA/NCSU-03-01-2536-NC.

## References

- [BBC<sup>+</sup>06] H.T. Banks, V.A. Bokil, D. Cioranescu, N.L. Gibson, G. Griso, and B. Miara. Homogenization of periodically varying coefficients in electromagnetic materials. *J. Sci. Comp.*, 28(2):191–221, 2006.
- [BG06a] H.T. Banks and N.L. Gibson. Electromagnetic inverse problems involving distributions of dielectric mechanisms and parameters. *Quart. Appl. Math.*, 64:749–795, 2006.
- [BG06b] H.T. Banks and N.L. Gibson. Void detection in foam with knit lines using THz pulse interrogation. *Math. Comp. Model.*, 44(9–10):807–815, 2006.
- [BGW05] H.T. Banks, N.L. Gibson, and W.P. Winfree. Gap detection with electromagnetic terahertz signals. *N. A.: Real World Apps.*, 6(2):381–416, 2005.

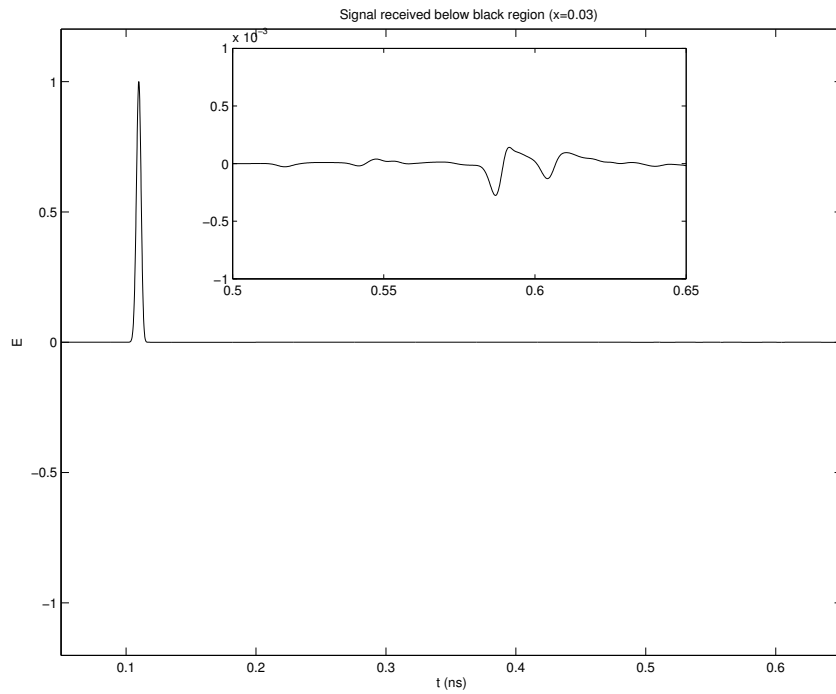


Figure 6: Shown is the difference between data received from non-normally incident, plane wave interrogating material *with and without a void* when receiver is placed *below* the low intensity region. (Note: original signal peak is shown for reference.)

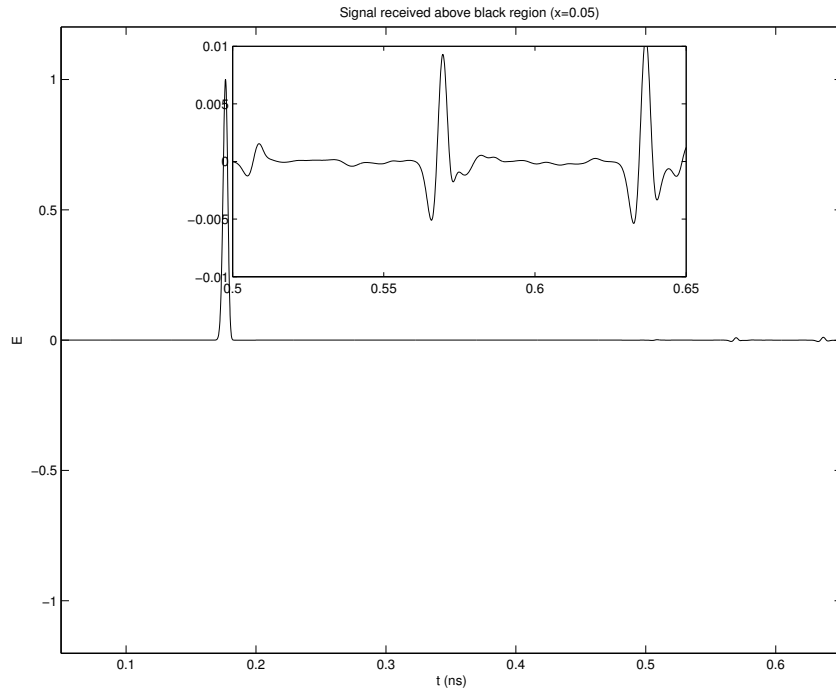


Figure 7: Shown is the difference between data received from non-normally incident, plane wave interrogating material *with and without a void* when receiver is placed *above* low intensity region. Amplitude of difference is two orders of magnitude larger.

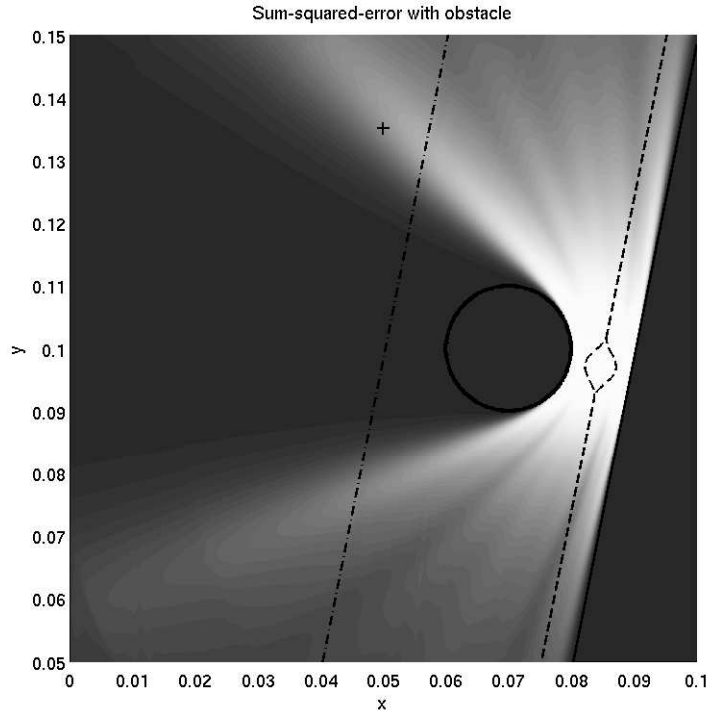


Figure 8: Shown is a surface plot of the objective function at  $w = 0$ . The cross denotes a location directly *above* the low intensity region. Note that it correlates with region of greatest contrast between material with void and without.

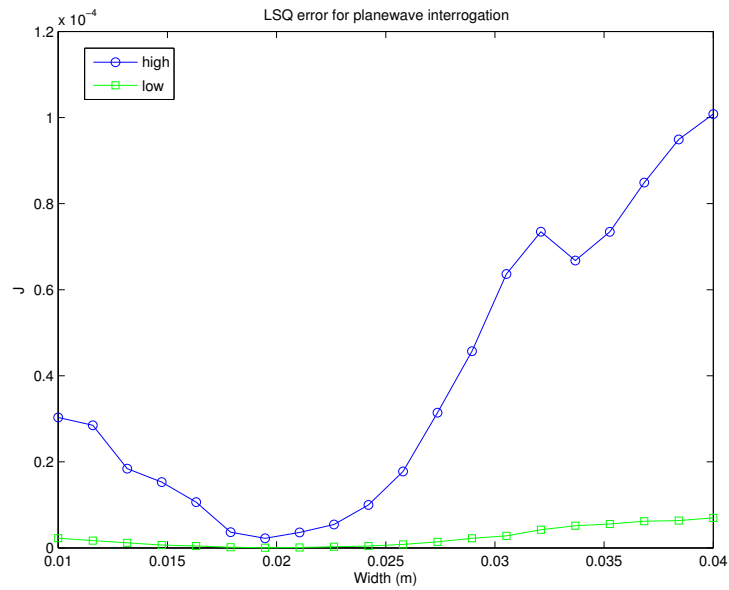


Figure 9: Objective function versus void size for two locations of receiver: above or below low intensity region.